

NEAR RECTILINEAR HALO ORBITS AND THEIR APPLICATION IN CIS-LUNAR SPACE

Emily M. Zimovan*, Kathleen C. Howell†, and Diane C. Davis‡

Near Rectilinear Halo Orbits (NRHOs), a subset of the L_1 and L_2 halo orbit families, are strong candidates for a future inhabited facility in cis-lunar space. Characteristics of the NRHOs, including stability and eclipsing properties, are presented along with a strategy to detect real-time diverging behavior. To be useful to future missions, the accessibility of these orbits must also be addressed. Transfer options from the NRHOs to the Distant Retrograde Orbits (DROs) are investigated. Additionally, a brief overview of past NRHO stationkeeping analysis is included.

INTRODUCTION

As evidenced by the Global Exploration Roadmap, international interest in a new era of human exploration of the solar system is emerging; cis-lunar space is a focus for the next phase.^{1,2} Operations in this extended Earth-Moon neighborhood will support space-based facilities for robotic and human missions to the Moon but also, eventually, to further destinations such as asteroids and Mars. To achieve this goal, a first step is the consideration of an inhabited facility in a long-term and relatively stable orbit in the lunar vicinity. One option for a habitat spacecraft in cis-lunar space is a Near Rectilinear Halo Orbit (NRHO).

Near rectilinear halo orbits are members of the broader set of L_1 and L_2 families of halo orbits, that is, foundational structures that exist in the dynamical environment modeled in terms of multiple gravitational bodies. The fundamental behavior also persists in a higher-fidelity model and, thus, supports potential long-term mission scenarios for spacecraft, possibly crewed, in orbits near the Moon.³ This type of trajectory was first identified in a simplified representation of the gravitational effects in the Earth-Moon system, i.e., the Circular Restricted Three Body Problem (CR3BP).^{4,5} In the CR3BP model, NRHOs are characterized by favorable stability properties that suggest the potential to maintain NRHO-like motion over a long duration while consuming few propellant resources. Some NRHOs also possess favorable resonance properties that can be exploited for mission design and are particularly useful to avoid eclipses.^{6,7} For actual mission implementations, however, transfers into such orbits, as well as stationkeeping strategies, must be demonstrated in a higher-fidelity ephemeris model.⁸ Stationkeeping algorithms for libration point orbits have previously been explored within this dynamical regime in the context of both planar Lyapunov and classical three-dimensional halo orbits.⁹ However, NRHOs as constructed in the ephemeris regime,

*Graduate Student, School of Aeronautics and Astronautics, Purdue University, Armstrong Hall of Engineering, 701 W. Stadium Ave., West Lafayette, IN 47907-2045. Member AAS; Member AIAA.

†Hsu Lo Distinguished Professor, School of Aeronautics and Astronautics, Purdue University, Armstrong Hall of Engineering, 701 W. Stadium Ave., West Lafayette, IN 47907-2045. Fellow AAS; Fellow AIAA.

‡Principal Systems Engineer, a.i. solutions, Inc., 2224 Bay Area Blvd., Houston, TX, 77058, USA. Member AAS.

characterized by nonlinear and sensitive dynamics, offer a more challenging problem since both high and low-cost solutions to the stationkeeping problem exist in close proximity. Thus, prediction of escape has recently emerged as an interesting aspect as well.⁷ The current investigation explores Earth-Moon NRHO properties that support NRHOs as a favorable type of orbit for a habitat facility in cis-lunar space and offers a summary of some recent analyses.

DYNAMICAL MODELS

As a basis for the construction of lunar near rectilinear halo orbits, dynamical models that supply different levels of fidelity are employed. The CR3BP provides an autonomous approximation to Earth-Moon dynamics, enabling an understanding of underlying dynamical structures. The ephemeris model allows for higher-fidelity simulation.

The Circular Restricted Three-Body Problem

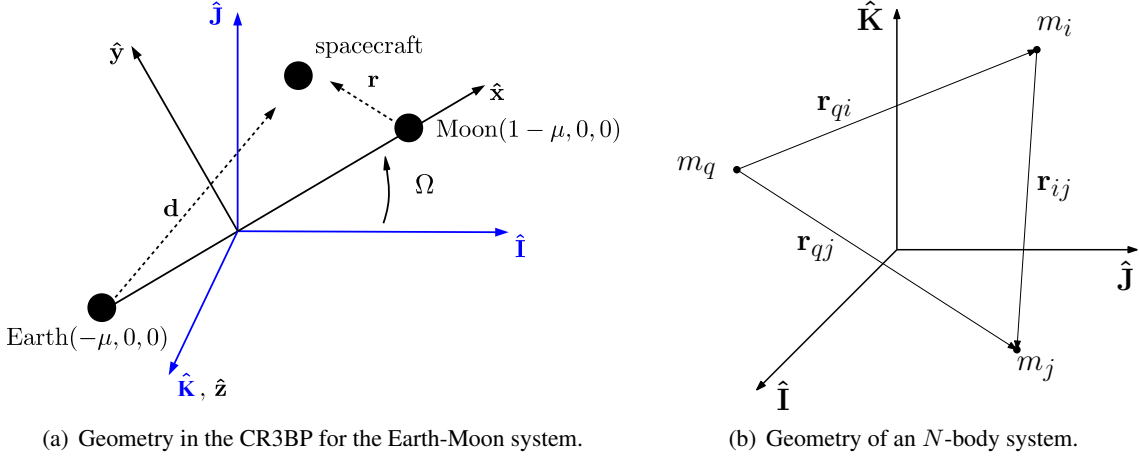
The dynamical model in the CR3BP serves as a reasonable approximation to higher-fidelity dynamical models in the Earth-Moon system, including those that may also incorporate solar gravity. Within this application of the CR3BP, the motion of a massless spacecraft under the gravitational influence of the Earth and Moon is considered. These two primary bodies, modeled as point-masses, are assumed to move in circular orbits about their common barycenter. The motion of the spacecraft is then described relative to a coordinate frame, $\hat{x}\text{-}\hat{y}\text{-}\hat{z}$, that rotates with the motion of the Earth and Moon as portrayed in Figure 1(a). In this frame, the spacecraft is located by the nondimensional coordinates (x, y, z) . By convention, quantities in the CR3BP are nondimensionalized such that the Earth-Moon distance, as well as the mean motion of the primaries, are both equal to a constant value of unity. In addition, the Earth and Moon masses are nondimensional and equal to $1 - \mu$ and μ , respectively, where the parameter μ equals the ratio of the mass of the Moon to the total mass of the system. In the rotating frame, then, the scalar equations of motion for the spacecraft are written as:

$$\ddot{x} - 2\dot{y} = \frac{\partial U}{\partial x}, \quad \ddot{y} + 2\dot{x} = \frac{\partial U}{\partial y}, \quad \ddot{z} = \frac{\partial U}{\partial z} \quad (1)$$

where the pseudo-potential function, $U = \frac{1}{2}(x^2 + y^2) + \frac{1-\mu}{d} + \frac{\mu}{r}$, while $d = \sqrt{(x + \mu)^2 + y^2 + z^2}$, and $r = \sqrt{(x - 1 + \mu)^2 + y^2 + z^2}$. The CR3BP admits five relative equilibrium points: the collinear points L_1 , L_2 , and L_3 , located along the Earth-Moon line, and two equilateral points, L_4 and L_5 , that form equilateral triangles with the two primaries. Since the CR3BP is autonomous, a constant energy integral exists in the rotating frame denoted the Jacobi constant, $JC = 2U - \dot{x}^2 - \dot{y}^2 - \dot{z}^2$. The existence of the Jacobi integral also introduces the Zero-Velocity Surfaces (ZVSs). In configuration space, these boundaries serve to define the regions of space that are accessible to the third body. Projecting the ZVSs into the x - y plane yields the Zero-Velocity Curves (ZVCs).¹⁰ As the value of the Jacobi constant decreases, accessible areas expand and the spacecraft can move throughout a larger region.

The Ephemeris Model

For applications such as mission planning, where higher-fidelity modeling accuracy is required, N -body differential equations and planetary ephemerides are employed. The dynamics to model the motion of N -bodies generally renders the motion of a particle of interest (e.g., a spacecraft), P_i , in an inertial frame $(\hat{\mathbf{I}}, \hat{\mathbf{J}}, \hat{\mathbf{K}})$ relative to a central body, P_q , under the gravitational influence of the same central body, P_q , and other perturbing particles, P_j . Such an N -body particle system is



(a) Geometry in the CR3BP for the Earth-Moon system.

(b) Geometry of an N -body system.

Figure 1. Reference frame definitions.

depicted in Figure 1(b). The well-known dimensional N -body relative vector equation of motion is written as

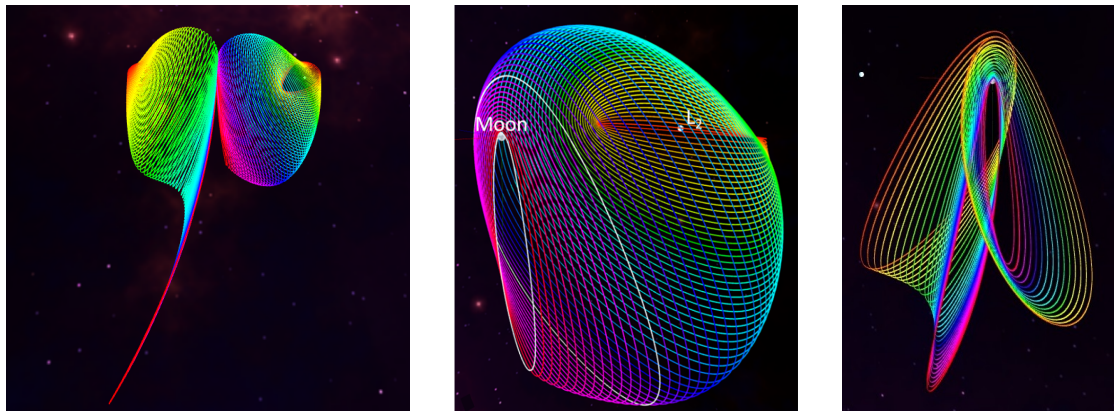
$$\ddot{\mathbf{r}}_{qi} = -G \frac{(m_i + m_q)}{r_{qi}^3} \mathbf{r}_{qi} + G \sum_{\substack{j=1 \\ j \neq i, q}}^N m_j \left(\frac{\mathbf{r}_{ij}}{r_{ij}^3} - \frac{\mathbf{r}_{qj}}{r_{qj}^3} \right) \quad (2)$$

where G denotes the universal gravitational constant, $m_{(\cdot)}$ is the mass of $P_{(\cdot)}$, and the definition of vector quantities is consistent with Figure 1(b). Note, a bold letter indicates a vector entity, while an identical non-bold symbol refers to the modulus of the corresponding vector. For this analysis, the relative position of each perturbing body with respect to the central body, \mathbf{r}_{qj} , is instantaneously computed by employing NASA's NAIF (Navigation and Ancillary Information Facility) SPICE ephemeris data. Since the operational trajectory for this specific analysis lies in proximity to the Moon, selecting the Moon as a central body is reasonable and convenient for numerical integration. For this application, the mass m_q in Figure 1(b) represents the Moon; the target mass, m_i , is the potentially crewed vehicle and the additional masses m_j correspond to additional bodies that exert a non-negligible gravitational attraction. The N -body vector differential equation is propagated in the J2000 inertial reference frame. Near the Moon, the Earth attraction, including the eccentricity of the Earth-Moon motion, and the tidal pull of solar gravity all significantly influence a trajectory at high altitude relative to the lunar surface. Accordingly, the Earth, Moon, and Sun are incorporated in an N -body ephemeris model. The largest planet in the solar system, Jupiter, is also included.

NEAR RECTILINEAR HALO ORBITS

Near rectilinear halo orbits⁴ in the vicinity of the Moon are identified as potential long-term orbits for a crewed vehicle in the cis-lunar region. The NRHOs offer advantages such as relatively inexpensive transfer options from the Earth, feasible transfer options to the lunar surface and other orbits in cis-lunar space and beyond, as well as advantageous eclipsing properties.^{3,8} The NRHOs represent a range of periodic halo orbits; the L_1 and L_2 families are depicted in Figure 2(a). The subsets that comprise the NRHOs are approximately bounded by specific locations reflecting changes in the linear stability across the corresponding halo family, that is, the bifurcations. The NRHO subset of

the L_2 halo family appears in Figure 2(b); the bounds are denoted in white. Representative NRHOs from both the L_1 and L_2 halo families are plotted in Figure 2(c) for comparison.*



(a) The L_1 and L_2 southern halo families of orbits in configuration space. (b) Zoomed-in view of the L_2 halo family delineating the bounds of the NRHOs in white. (c) Zoomed-in view of the L_1 and L_2 NRHOs.

Figure 2. The L_1 and L_2 halo orbit families and the NRHOs.¹¹

A family of related periodic orbits bifurcates, in fact, from the L_2 near rectilinear halo orbits; members of this family appear in Figure 3. In appearance, the members of this family represent a “butterfly” in shape; specifically, this family of orbits bifurcates from a particular NRHO that has a period of approximately 6 days.⁹ The butterfly family of orbits possesses characteristics similar to those of the near rectilinear halo orbits offering similar advantages for trajectory design in this vicinity. Of note, comparable motions in the vicinity of the smaller primary in the CR3BP were documented as early as 1980 by Robin and Markellos and examined in 1993 by Stringer and Richardson.^{5,12} The motion in a butterfly orbit resembles a “figure-8” shape, however, these orbits wrap around both the near and far side of the Moon, as apparent in Figure 3.



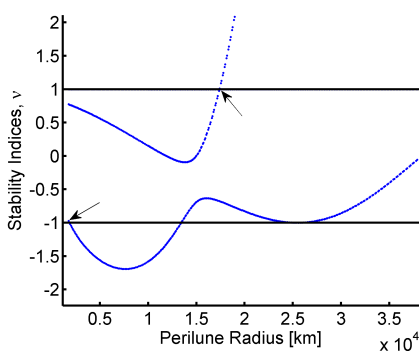
Figure 3. The southern butterfly family of orbits as viewed in configuration space.¹¹

*Visuals enabled by Davis et al.¹¹

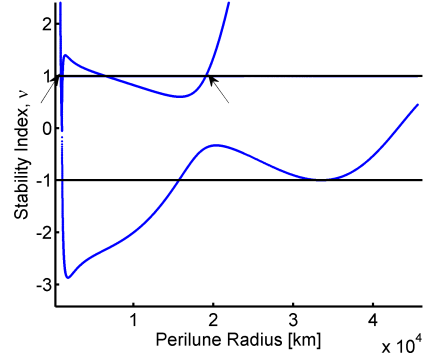
Stability

Within the context of the CR3BP, it is relatively straightforward to determine the linear stability associated with periodic orbits. Linear stability for a periodic solution in any autonomous dynamical system is assessed via the eigenvalues of the State Transition Matrix (STM) evaluated after precisely one periodic interval, i.e., the monodromy matrix. The STM is essentially a linear mapping and reflects the convergence or divergence of variations relative to a reference solution. Two well-known properties of the monodromy matrix, as applied within the context of the CR3BP, are necessary to analyze the stability of NRHOs: (1) The eigenvalues of the monodromy matrix always appear in reciprocal pairs, and (2) one pair of eigenvalues is always equal to unity due to the periodicity of the orbit and the existence of a family of such orbits with precisely periodic behavior. Excluding the trivial pair, two reciprocal pairs of eigenvalues, $(\lambda_i, 1/\lambda_i)$, are combined into a single metric for the purpose of describing the stability of the corresponding mode. A stability index is then defined as $\nu_i = \frac{1}{2}(\lambda_i + 1/\lambda_i)$ for $i = 1, 2$. If the stability indices, ν_i , are both less than one in modulus, then the orbit is marginally stable in a linear sense; the orbit is otherwise unstable. For a diverging path, a larger value of the stability index corresponds to a faster departure from the reference.

The linear stability characteristics associated with the halo families of periodic orbits in the CR3BP serve to delineate the NRHO boundaries by delivering distinct markers that bound the NRHO region of orbits. Across the L_1 and L_2 halo families, in the region of interest near the smaller primary, a number of stability switches, or transitions, occurs from marginally stable to unstable or vice versa. The NRHOs are defined as the subsection of the halo orbit family possessing stability indices all within some small bound surrounding ± 1 and with no stability index that is significantly larger in magnitude than the others. Thus, for the purposes of this investigation, an L_2 NRHO is defined, in the Earth-Moon system, as a halo orbit between the first and third stability changes in the region of the smaller primary, marked with arrows in Figure 4(a). The L_1 NRHOs are defined as the orbits between the first and fourth stability changes within the Earth-Moon system, marked with arrows in Figure 4(b).



(a) Stability index across the L_2 halo family.



(b) Stability index across the L_1 halo family.

Figure 4. The region of bounded stability index values defines the interval across the halo orbits that are debited as NRHOs.

The definition for the NRHO interval along the L_1 and L_2 families of halo orbits equivalently applies to both the northern and southern members. The orbital geometry also distinguishes an NRHO from the larger set of halo orbits; the NRHOs are characterized by an elongated shape that

resembles an ellipse when it is plotted in the CR3BP rotating frame; the orbits are also dominated by the out-of-plane components. Earth-Moon L_2 NRHOs are characterized by perilune radii ranging from approximately 1850 km to 17350 km. (Recall that the lunar radius is approximately 1737 km.) The orbital periods across the L_2 NRHOs range from approximately 6 days to just over 10 days, as evident in Figure 5(a). The L_1 NRHOs possess perilune radii ranging from approximately 900 km to 19000 km with periods between approximately 8 days and 10 days, as plotted in Figure 5(a). The Jacobi constant values for the L_1 and L_2 halo families appear in Figure 5(b).

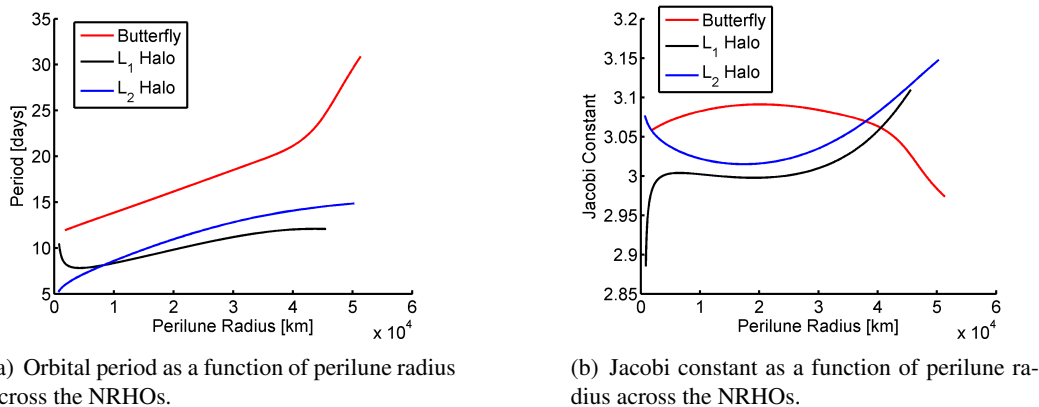
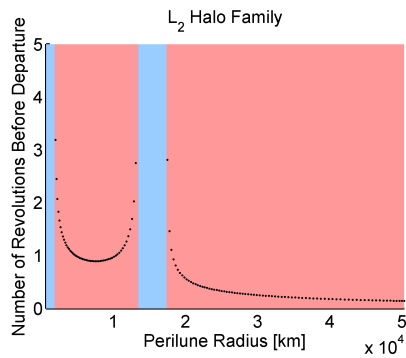


Figure 5. Characteristic parameters as a function of perilune radius for the NRHOs in the CR3BP.

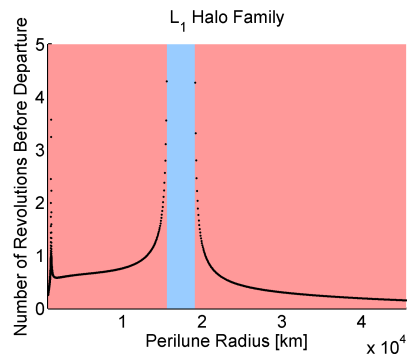
Any NRHOs with stability indices such that $|\nu_i| > 1$ are unstable. The divergence rate is, however, significantly slower than for other halo orbits that are closer to the L_2 or L_1 Lagrangian points, as evaluated in the Earth-Moon system. The temporal scale for the divergence reflecting the instability is roughly predicted by the modulus of the stability index. When both of the stability indices are close to unity in terms of the modulus, e.g., corresponding to an NRHO, divergence is slow. Within the NRHO range, both stability indices remain bounded and nearly equal to one. A reference metric for the temporal scale of the dominant diverging motion is derived by considering the time constant, τ , as measured in the number of revolutions of the nominal orbit, that is

$$\tau[\text{rev}] = \frac{1}{|\text{Re}(\ln(\lambda_{\max}(\Phi(P, 0))))|} \quad (3)$$

where $\lambda_{\max}()$ is an operator that returns the largest eigenvalue of the argument matrix and $\Phi(P, 0)$ denotes the STM over precisely one period (P) of the orbit. Note that the time constant is infinite for a marginally stable orbit, i.e., $\lambda_{\max}(\Phi(P, 0)) = 1$. The value τ is physically interpreted as the time interval necessary to amplify a given initial perturbation by a factor of approximately 3, assuming that the growth is proportional to the exponential function $e^{\frac{t[\text{rev}]}{\tau[\text{rev}]}}$. The time constant associated with the range of NRHOs is displayed in Figure 6. Favorable stability properties and the time scale of divergence as observed in the CR3BP suggest the possibility of maintaining NRHO motion over a long duration while consuming few propellant resources. Leveraging this opportunity does require the introduction of a stationkeeping algorithm to maintain NRHO-like motion in a higher-fidelity environment. The butterfly family possesses stability properties similar to the NRHOs. As is apparent in Figure 7(a), the butterfly orbits are either stable or nearly stable (in a linear sense) over the range of the family consistent with perilune radii similar to those in the NRHO range of orbits in the halo families. When unstable, the butterfly orbits have a slightly higher rate of



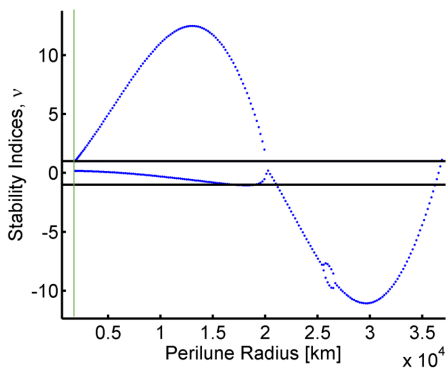
(a) Time constant as a function of perilune radius across the L_2 NRHOs.



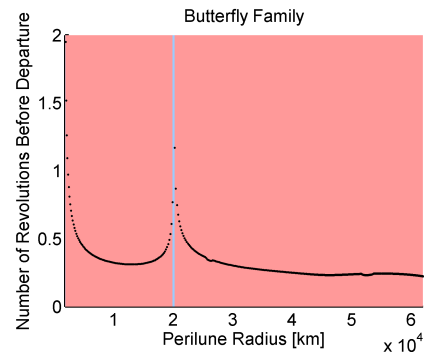
(b) Time constant as a function of perilune radius across the L_1 NRHOs.

Figure 6. Linear time constant for the NRHO regions within the Earth-Moon system. Blue regions indicate marginally stable orbits; red regions denote unstable orbits.

divergence than that of the NRHOs, as indicated by the larger value of the stability index and the time constant in Figure 7(b). In Figure 7(a), the stability index corresponding to the orbit that marks the period doubling bifurcation from the NRHOs is marked with a green line. Additional characterizing information concerning the butterfly family is included in Figure 5. Note that the periods of the butterfly orbits are approximately twice that of the NRHOs, not surprising considering their geometry. The corresponding Jacobi constant values appear to deliver an opposing trend, i.e., the maximum Jacobi constant for the butterfly family approximately occurs at the local minimum of the Jacobi constant curve for the halo families.



(a) Stability index across the butterfly family. The green line locates the orbit that bifurcates from the L_2 NRHOs.



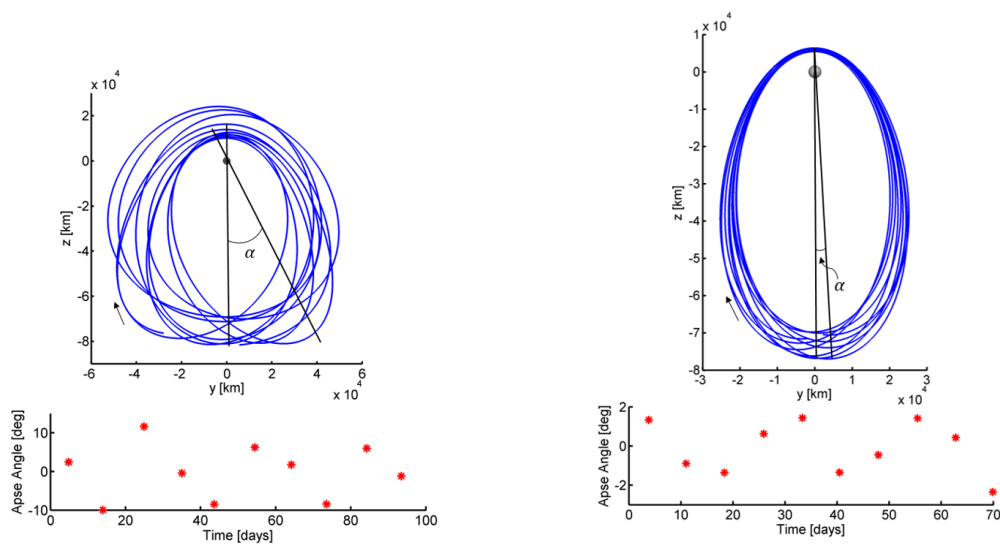
(b) Linear time constant as a function of perilune radius across the family of butterfly orbits. Blue regions indicate marginally stable orbits; red regions denote unstable orbits.

Figure 7. Stability characteristics of the butterfly family of orbits.

Apse Angle

Given periodic orbits such as NRHOs in the CR3BP, transition to a higher-fidelity ephemeris force model yields quasi-periodic behavior. The transition can result in either “tight,” nearly-periodic orbits or “loose,” more variable revolutions along a trajectory path. A metric is defined for convenience

to describe the spread of the orbit given a perfectly periodic CR3BP analog. The metric is denoted the apse angle, α , and is depicted in Figure 8. The apse angle reflects the ‘excursion’ of a series of



(a) An ephemeris trajectory with a wider spread relative to a corresponding CR3BP orbit, as determined by the large range of the apse angle and the “loose” appearance in the Earth-Moon rotating frame.

(b) An ephemeris trajectory with a narrow spread that remains close to a corresponding CR3BP orbit, as determined by the small range of the apse angle and the “tight” appearance in the Earth-Moon rotating frame.

Figure 8. Computation of the apse angle to quantify the evolution of a converged ephemeris trajectory in comparison to a corresponding CR3BP NRHO.

revolutions along an ephemeris trajectory, i.e., it is a measure of the degree to which one revolution mirrors the previous revolution. For application to the NRHOs, the apse angle tracks the evolution of an ephemeris trajectory, relative to a periodic NRHO computed in the CR3BP, in terms of its orientation in the yz -plane. By definition, a CR3BP periodic NRHO retains a constant apse angle, $\alpha = 0^\circ$. The apse angle is then evaluated as the osculating argument of periapsis, computed at the closest approach of the ephemeris path relative to the Moon (minus 90°); thus, it is evaluated once every revolution. Figure 8(a) reflects the fact that the apse angle along a converged ephemeris trajectory can vary widely; this is illustrated by the 3:1 synodic resonant NRHO converged using only a continuity constraint in the figure. Alternatively, as is apparent in Figure 8(b), some ephemeris NRHOs closely resemble their CR3BP counterparts. Additionally, since the NRHOs in Figures 8(a) and 8(b) are, in fact, a 3:1 synodic resonant orbit and a 4:1 synodic resonant orbit, respectively, some cyclic behavior in the apse angle is clearly observed in the plots of α in Figures 8(a) and 8(b). The plots also serve to identify the resonances when visual inspection, e.g., in Figure 8(a), may not reveal any obviously repeating behavior.

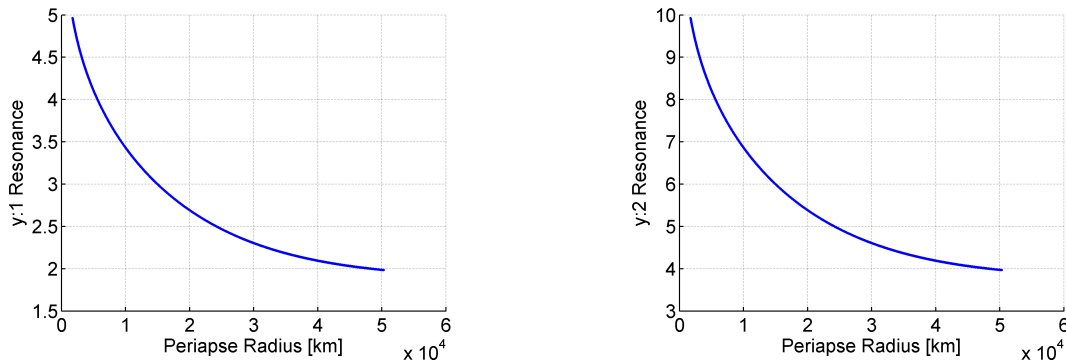
Eclipsing

Mission constraints due to limitations on spacecraft temperature and time without a direct communications link to Earth dictate allowable eclipse duration and frequency.⁸ Spacecraft in NRHOs are subject to both Earth eclipse and lunar eclipse conditions due to their proximity to both of these primary bodies. Trajectory design strategies to minimize shadow event durations are explored in

this preliminary analysis.

Orbital resonance is an important consideration for meeting eclipse constraints. Both sidereal and synodic resonances between a vehicle in an NRHO and the Moon are considered. Resonance in terms of a sidereal period is focused on the time required for a celestial body to complete one revolution (360 degrees) in its orbit relative to another body. For example, a viewer fixed in the center of Earth would see the Moon return to the same location in the sky after one sidereal period of the Moon. The Moon's sidereal period is approximately 27.322 days. Resonance in terms of the synodic period is focused on the time between successive conjunctions of a celestial body with the Sun. In this case, a viewer fixed in the center of Earth would see the Moon return to the same location with respect to the Sun after one synodic period of the Moon, however, the Moon would *not* appear in the same location in the sky. The Moon's synodic period is approximately 29.5306 days, slightly longer than its sidereal period.

Due to the fact that avoiding long duration eclipses is typically an important mission criteria, the location of the Earth and Moon with respect to the Sun and, therefore, the synodic resonance, is a priority. In Figure 9, the y:1 and y:2 synodic resonances for various L_2 halo orbits as computed in the CR3BP are plotted as a function of perilune radius. The ratio y:n reflects the number, y, of

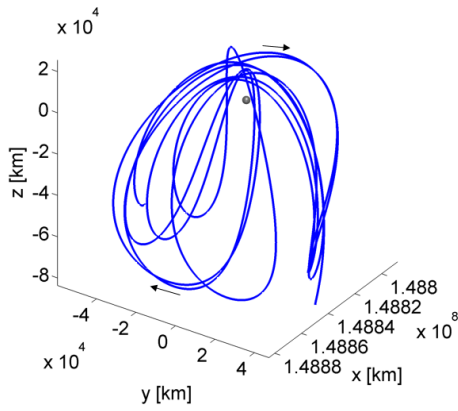


(a) The y:1 synodic resonance indicates that the spacecraft completes y revolutions of the halo orbit in one lunar synodic period.

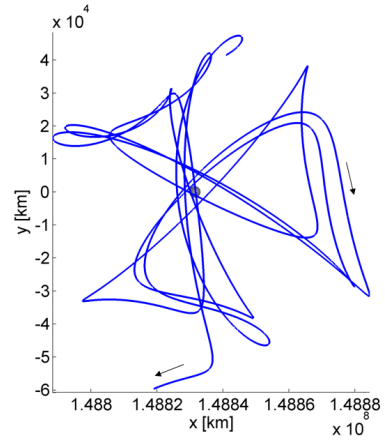
(b) The y:2 synodic resonance reflects a spacecraft that completes y revolutions of the halo orbit in two lunar synodic periods.

Figure 9. Synodic resonance of the L_2 halo family as a function of perilune radius.

completed revolutions along a specific halo orbit per n synodic cycles of the Moon, respectively. For example, a 4:1 synodic resonance, that occurs for an NRHO with perilune radius of about 5600 km, indicates that four revolutions of the NRHO are completed over one lunar synodic period. A 3:1 synodic resonance occurs for an NRHO with perilune radius equal to approximately 15000 km, while the 9:2 resonant NRHO possesses a perilune radius of about 3150 km. The 3:1 synodic resonant orbit, as computed in the ephemeris model, appears in Figure 10 in the Sun-Moon rotating frame. The Sun-Moon rotating frame is selected to visualize this orbit since the resonance becomes apparent in this view. Since the period of this NRHO is one third of the lunar synodic period, three distinct lobes appear in the Sun-Moon Rotating frame. Similarly, for a y:1 synodic resonant orbit, y distinct lobes are observed. For y:2 synodic resonant orbits, y lobes appear, but the path encompasses the Moon twice rather than once, as is the case for y:1 synodic resonant orbits. In the Sun-Moon rotating frame, the Moon's shadow is fixed in the positive x -direction. With careful epoch selection, eclipses can thus be avoided by aligning the lunar shadow with gaps in the tra-



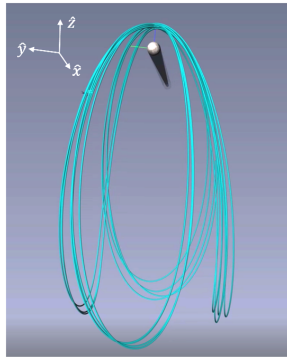
(a) A 3:1 synodic resonant NRHO as viewed in three dimensions in the Sun-Moon rotating frame.



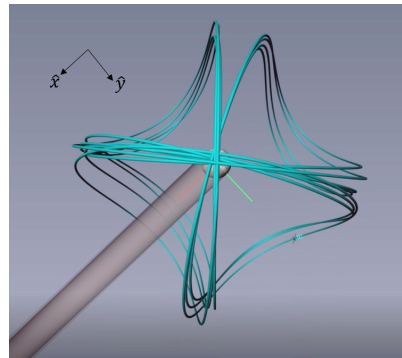
(b) A 3:1 synodic resonant NRHO as observed looking down the z -axis onto the x - y plane, in the Sun-Moon rotating frame.

Figure 10. Ten revolutions of a 3:1 synodic resonant NRHO computed in the ephemeris model shown in the Sun-Moon rotating frame.

jectory, since changing the date of insertion into the NRHO essentially rotates the trajectory in the Sun-Moon rotating frame. In Figure 10, for example, a 3:1 synodic resonant NRHO is aligned such that a large gap in the orbit lies along the positive x -axis in the Sun-Moon rotating frame, and thus, lunar eclipse events are avoided. Similarly, in Figure 11, a sample 4:1 synodic resonant NRHO, as computed in the higher-fidelity ephemeris model, is plotted in the Sun-Moon rotating frame; an insertion epoch is selected such that all lunar eclipse events are avoided. Although the insertion epoch can be selected to avoid lunar eclipse events, eclipses due to the Earth's shadow are also a concern. However, due to the geometry of the NRHOs, if the spacecraft apoapsis occurs during each full Moon phase, passage through the Earth's shadow is also avoided.



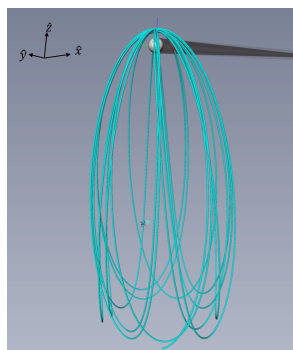
(a) A 4:1 synodic resonant NRHO shown in three dimensions.



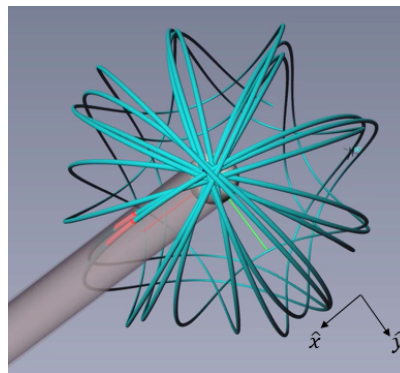
(b) A 4:1 synodic resonant NRHO shown looking down the z -axis onto the x - y plane.

Figure 11. The shadow of the Moon passes through a large gap in the trajectory, completely eliminating lunar eclipse events.

As an example of a trajectory that does encounter lunar eclipse events, a 9:2 synodic resonant orbit is plotted in Figure 12. Consistent with the 4:1 trajectory in Figure 11, the 9:2 synodic resonant path in Figure 12 is constructed in the ephemeris model. The lunar shadow does not cleanly pass through the narrow gaps in the orbit and, therefore, two lunar eclipse events result as highlighted in red. Each of these eclipse events is about 60 minutes in duration. Carefully selecting an insertion date can, in fact, eliminate the lunar eclipsing in this trajectory, however, due to the narrow trajectory gaps, epoch date selection may be more challenging than in the case of the 4:1 synodic resonant NRHO.



(a) A 9:2 synodic resonant NRHO shown in three dimensions.



(b) A 9:2 synodic resonant NRHO shown looking down the z -axis onto the x - y plane.

Figure 12. The shadow of the Moon encounters a portion of the trajectory, noted in red.

Escape Warning

For any application involving a spacecraft in an orbit such as an NRHO, orbit maintenance is required. The potential to anticipate, or predict, an escaping path, i.e., an “escape warning” is useful in this regime, particularly if escape can be predicted prior to any visual evidence of any apparently diverging states. Thus, a simple quantity to detect an escape with a sufficient time margin is a key capability. Initially, consider the following scalar quantity along a trajectory constructed in the CR3BP that was previously introduced by Guzzetti et al.,⁶ i.e.,

$$\text{MI}_{\Gamma}(t) = \int_{t_0}^t x(\tilde{t})\dot{x}(\tilde{t}) + y(\tilde{t})\dot{y}(\tilde{t}) + z(\tilde{t})\dot{z}(\tilde{t})d\tilde{t} \quad (4)$$

where x , y , z are the position coordinates relative to the rotating frame and \dot{x} , \dot{y} , \dot{z} are the corresponding velocity components, all functions of a single independent time variable, \tilde{t} . The quantity $\text{MI}_{\Gamma}(t)$ is termed the momentum integral by Guzzetti. The expression in Eq. (4) is effectively a line integral for the position vector field computed between the initial epoch, t_0 , and current epoch, t . The momentum integral along a closed orbit is equal to the circulation of the position vector as observed in the CR3BP rotating frame. Given a precisely periodic orbit as computed in the CR3BP, the momentum integral, as evaluated over one period, is zero. An example (from Guzzetti et al.⁶) appears in Figure 13(a). The momentum integral evolves along an NRHO in the CR3BP with perilune radius equal to 3500 km. After one revolution of the orbit, $\text{MI}_{\Gamma}(t)$ returns to zero, as demonstrated in Figure 13(a). There are no restrictions on the application of the momentum integral

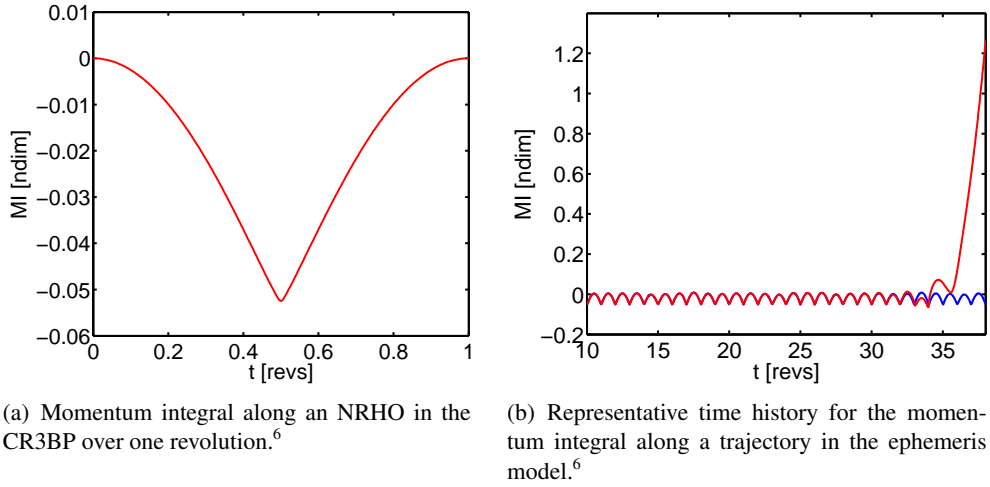


Figure 13. Momentum integral in the CR3BP (a) and ephemeris model (b)

to any pre-determined model or level of fidelity. Thus, the process can be employed in a higher-fidelity ephemeris model, for example. For an NRHO trajectory constructed in the ephemeris model, the orbit is not periodic and does not return to the initial point. As a consequence, the momentum integral evaluated over one revolution does not equal zero. However, as the path evolves through many revolutions, if $MI_{\Gamma}(t)$ remains bounded, then the path remains bounded. Thus, for a quasi-periodic trajectory or an NRHO orbit in the ephemeris model, the momentum integral oscillates within acceptable bounds.

Guzzetti et al. compare the momentum integral profile for a baseline trajectory to a slightly perturbed path that departs from the reference orbital path. For this scenario, the time history for the momentum integral is plotted in Figure 13(b). The blue curve, representing the nominal path, is bounded and approximately repeats over each revolution. The red curve reflects a perturbed trajectory. After approximately 30 revolutions, the divergence of the perturbed path is apparent. As the departure evolves, the momentum integral profile is no longer bounded and does not approximately repeat over each revolution of the nominal orbit. Given the result in Figure 13(b), one possible metric to detect divergence is the instantaneous difference between the momentum integral computed for a perturbed trajectory versus a given long-term baseline trajectory. Define the difference as

$$\Delta MI(t) = \log |MI_{\tilde{\Gamma}}(t) - MI_{\Gamma}(t)| \quad (5)$$

where $\tilde{\Gamma}$ refers to the perturbed trajectory and Γ refers to the reference orbit; a logarithm function reveals the order of magnitude for the momentum integral difference.

From Guzzetti et al., a valid instantaneous variation, along a logarithmic scale, for a perturbed momentum integral (red curve in Figure 13(b)) relative to a baseline profile (blue curve in Figure 13(b)) appears in Figure 14(a). When the orbital motion begins diverging, the order of magnitude of ΔMI rises quickly. In Figure 14(a), the vertical line indicates where the osculating eccentricity relative to the Moon is equal to unity. Monitoring of the momentum integral difference offers an approach to predict, with a sufficient time margin, the divergence of the possibly perturbed current trajectory relative to the baseline or reference motion. For the sample NRHO in Figure 14, $\Delta MI(t)$ allows for a prediction consistently 4–6 revolutions ahead of an escaping path, as seen in Figure 14(b). A stationkeeping strategy can leverage such information.

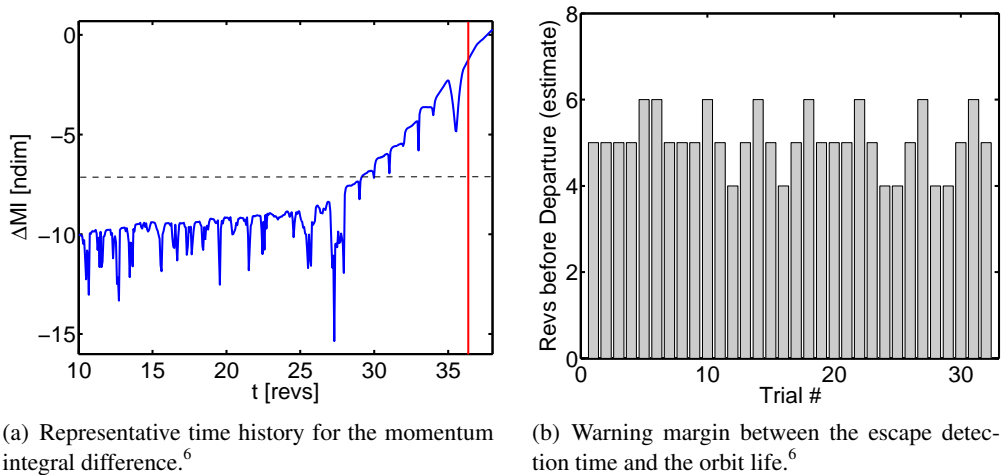


Figure 14. Escape prediction using the momentum integral difference.

TRANSFER TRAJECTORIES

To assess the accessibility and applicability of NRHOs to missions in cis-lunar space, preliminary transfer trajectories to and from these periodic orbits are constructed. As with any spacecraft departing from Earth, transfer options from Low Earth Orbit (LEO) to the orbit of interest, that is, the NRHOs, is an important first step. To be useful, the NRHOs must be accessible from LEO for a reasonable cost and time of flight. Additionally, since the NRHOs serve as a potential staging orbit in cis-lunar space, access to other orbits in the vicinity is also a consideration. One type of transfer that has been a recent focus is a path from an NRHO to a Distant Retrograde Orbit (DRO).

Accessing Near Rectilinear Halo Orbits from Low Earth Orbit

To access the NRHOs from the Earth, a departure from LEO is investigated. To support this preliminary transfer investigation, a 4:1 synodic resonant NRHO is selected as the baseline orbit. Here, a departure from a 200 km altitude orbit about the Earth is considered. The NRHO arrival is constrained to be tangential and located at apolune along the NRHO. Apolune is intentionally selected for the arrival location due to its low sensitivity as compared to perilune; low sensitivity is preferred from a navigational standpoint. One straightforward direct transfer option is plotted in Figure 15. The time of flight corresponding to this transfer is 5.33 days and the impulsive departure from LEO is 3.124 km/s. The capture into the NRHO requires 0.829 km/s, resulting in a total cost of 3.953 km/s. Such a ΔV estimate is reasonable and comparable to other transfers that arrive in the lunar vicinity.¹³ This preliminary transfer also accommodates inclination; the sample transfer in Figure 15 departs a LEO orbit with an inclination of approximately 28 degrees. While many transfer geometries are possible, the specific geometry observed in Figure 15 is reasonably low-cost, direct, and short duration, characteristics that are preferable for crewed missions. Additionally, this transfer geometry has relatively low sensitivity given that the majority of the path remains far from the primary bodies resulting in desirable navigational characteristics. Using a continuation scheme, a similar transfer geometry from LEO to individual members of the L_2 NRHO family is constructed. The characteristics of this family of transfers is summarized in Figure 16. Preliminary results determined in the CR3BP support the assumption that transfers from LEO to representative NRHOs are feasible and consistent with other such direct transfer orbits. Alternative transfer scenarios have also

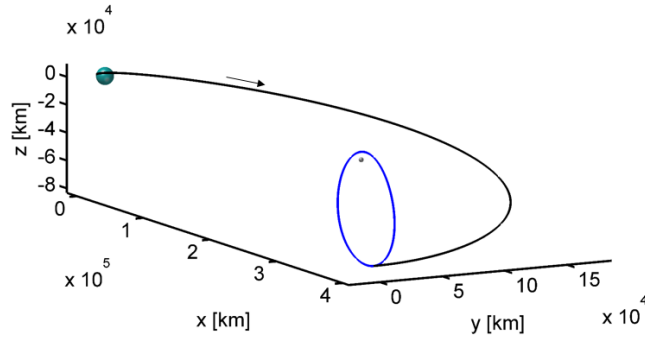


Figure 15. A simple transfer from a 200 km altitude LEO to apolune on the 4:1 synodic resonant L_2 NRHO, as computed in the CR3BP.

been suggested, for example, incorporating lunar flybys.⁸ Additional investigations are ongoing.

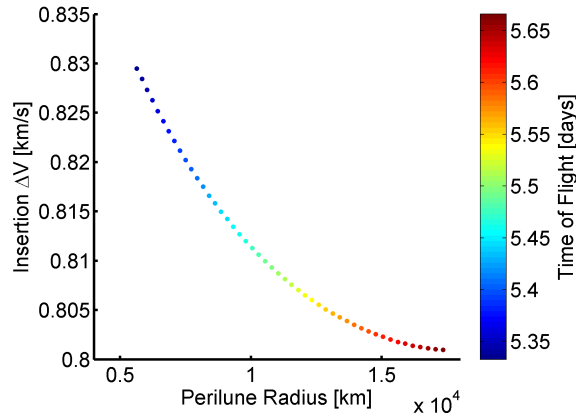
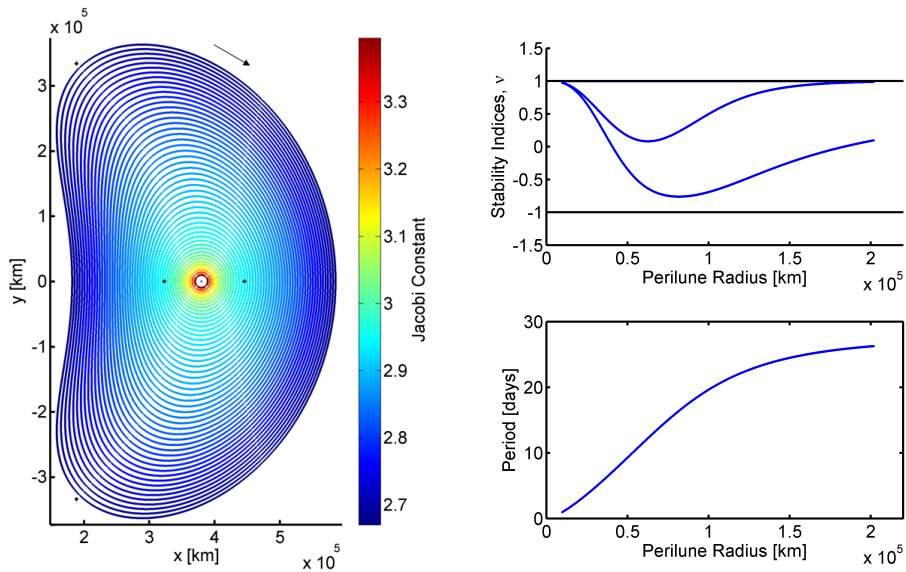


Figure 16. Characteristics for transfers from LEO to apolune on the L_2 NRHOs for the geometry shown in Figure 15.

Accessing Distant Retrograde Orbits

The Distance Retrograde Orbits (DROs) are a stable family of planar periodic orbits about the smaller primary; this family of orbits exists as a fundamental orbit type in the CR3BP. These DROs represent desirable orbits in cis-lunar space due to the low variation in sensitivity over each revolution. The concept and computation of the DRO family is not new and has been examined by various authors beginning in the 1960s. For example, the existence of the DROs in the Earth-Moon system as planar periodic retrograde orbits about the Moon were introduced as family “C” by Broucke in 1968.¹⁴ Notable work by Hénon in the Hill problem contributed to the dynamical understanding of the DROs, which were denoted as family “f” in that work.¹⁵ A sampling of representative DROs and their associated stability indices are plotted in Figure 17. The DROs were recently considered in support of the proposed Asteroid Redirect Mission (ARM).¹⁶ As NRHOs have emerged as potential habitat locations, links between such families of orbits are a subject of current interest.

Transfer trajectories from the NRHOs to the DROs are particularly challenging due to the relative stability of each orbit in these families and the resulting lack of useful manifold arcs.¹³ Additionally,

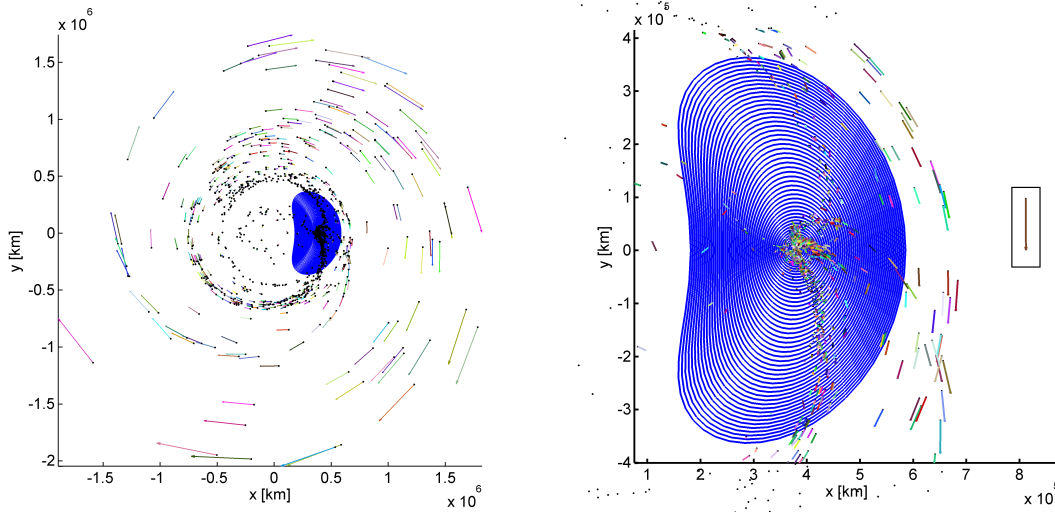


(a) Distant Retrograde Orbits (DROs) about the Moon colored by Jacobi constant. The Lagrange points are marked in black. (b) Stability indices and period as a function of perilune radius across the DRO family.

Figure 17. Planar periodic DROs about the Moon.

the required plane change of almost 90 degrees further increases the complexity. To construct pathways from the NRHOs to the DROs, a Poincaré mapping strategy is employed. Poincaré maps are a powerful trajectory design tool that allows for wide-ranging trajectories to be concisely visualized by reducing the dimension of the dynamical system.¹⁰ To generate the Poincaré map used in this investigation, a hyperplane is selected at $z = 0$. Each crossing of the hyperplane is recorded on a plot as the x - y coordinate of the crossing. To supply additional information in the map concerning the 6-dimensional state at the plane crossing, a glyph is added, i.e., an arrow in the direction of (\dot{x}, \dot{y}) is added to the plot with a length corresponding to the inverse of the magnitude of the \dot{z} value at the hyperplane. The initial conditions for each propagated trajectory is generated by introducing a maneuver of magnitude 0.051 km/s at apoapsis along the 4:1 synodic NRHO in various directions on a unit sphere. Figure 18 illustrates the resulting Poincaré map with the DRO family included for completeness.

For a transfer from an NRHO to a DRO, determined via differential corrections techniques, a trajectory segment selected from the Poincaré map serves as an initial guess. The segment is identified by a map crossing near a sample DRO of interest. A candidate crossing is close to the DRO in (x, y) position space, and the in-plane velocity direction, as illustrated by the orientation of the glyph, is directed in approximately the same direction as the velocity along the DRO. Additionally, a small \dot{z} component at the crossing, indicated by a longer arrow on the map, is desired. One such crossing is highlighted in a box in Figure 18(b). This crossing corresponds to an initial maneuver in the CR3BP rotating frame of $\Delta \mathbf{V} = -0.0396\hat{x} - 0.0043\hat{y} - 0.0318\hat{z}$ km/s at apolune on the NRHO and requires a time of flight of approximately 60 days. Exploiting the trajectory segment from the map as a starting point, a transfer from the 4:1 synodic resonant NRHO to a 26.3 day period DRO is constructed, and plotted in Figure 19.



(a) Poincaré map with departure maneuver equal to 0.051 km/s at apoapsis on the NRHO.

(b) Zoomed-in view of the DRO region.

Figure 18. A Poincaré map is used to find a viable initial guess for a transfer trajectory from the NRHOs to the DROs.

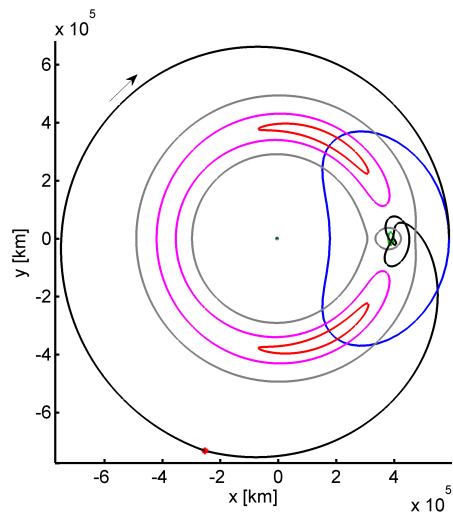
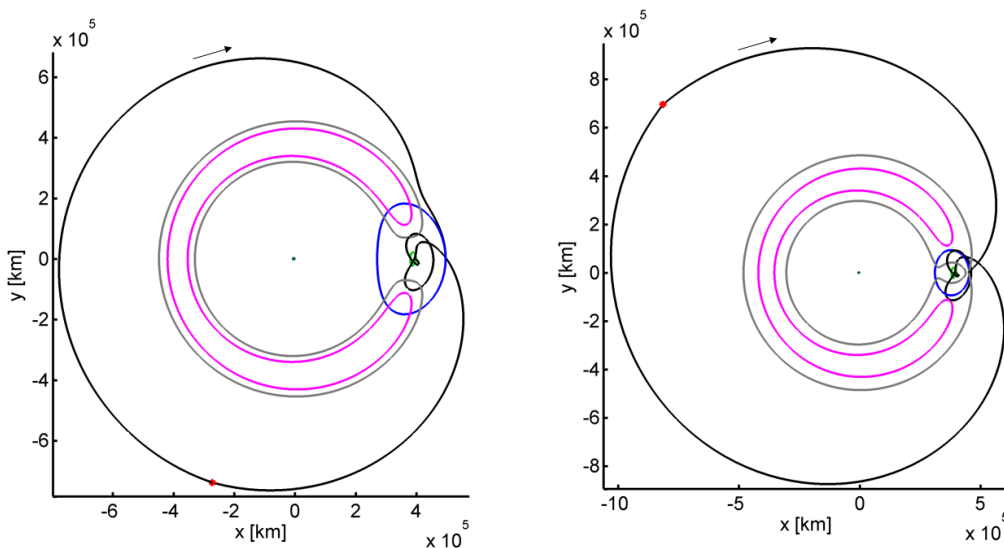


Figure 19. Transfer from the 4:1 synodic resonant NRHO to a 26.3 day period DRO.

The transfer in Figure 19 includes an intermediate maneuver, marked with a red star along the trajectory path. The total cost for this transfer is 0.7310 km/s with a time of flight of 74.2627 days. The ZVCs for each trajectory segment (corresponding to different values of Jacobi constant along each segment) are also plotted in the figure. For this transfer geometry, the ZVC for the Jacobi constant value corresponding to the NRHO appears in magenta; the ZVC for the Jacobi constant value associated with the transfer segment between the departure maneuver on the NRHO and the intermediate ΔV is plotted in red; and, the grey curves represent the ZVC for the Jacobi constant value computed for the transfer segment between the intermediate ΔV and the arrival

maneuver at the DRO. The ZVC for the DRO is not included in the figure as the corresponding ZVS is out-of-plane and curves do not appear in the x - y plane (i.e., $JC_{DRO} > JC_{L_4}$). Using a continuation scheme, this transfer geometry recurs for transfers to smaller DROs in the family. Two additional examples appear in Figure 20. In Figure 20(a), a transfer to a smaller, 20.97 day period DRO is constructed; the time of flight is then 80.8 days and the total cost of the maneuvers is equal to 0.5799 km/s. A transfer to a second, even smaller, DRO with period 13.76 days appears in Figure 20(b) with a time of flight of 75.5 days and a total ΔV equal to 1.206 km/s. As the size of the DRO changes, the Jacobi constant along each transfer segment changes. The transfer in Figure 19 is observed to include no interaction with the ZVCs, while the transfers in Figure 20 do approach and seemingly “bounce off” of the ZVC resulting in a slightly modified geometry. The outer transfer segment in Figure 20(b) apparently expands in size to accommodate the ZVC corresponding to the trajectory segment between the intermediate and arrival maneuvers (shown in grey) as the L_2 gateway closes. As such, the location of the intermediate ΔV shifts to a positive \hat{y} value. Interestingly, the transfer segment between the departure maneuver and the intermediate impulsive ΔV decreases in Jacobi constant value and associated the ZVC (in red in Figure 19) disappears from the x - y plane. While many transfer geometries between the NRHOs and DROs are possible, this geometry suggests transfer-ZVC interactions that influence the transfer characteristics.

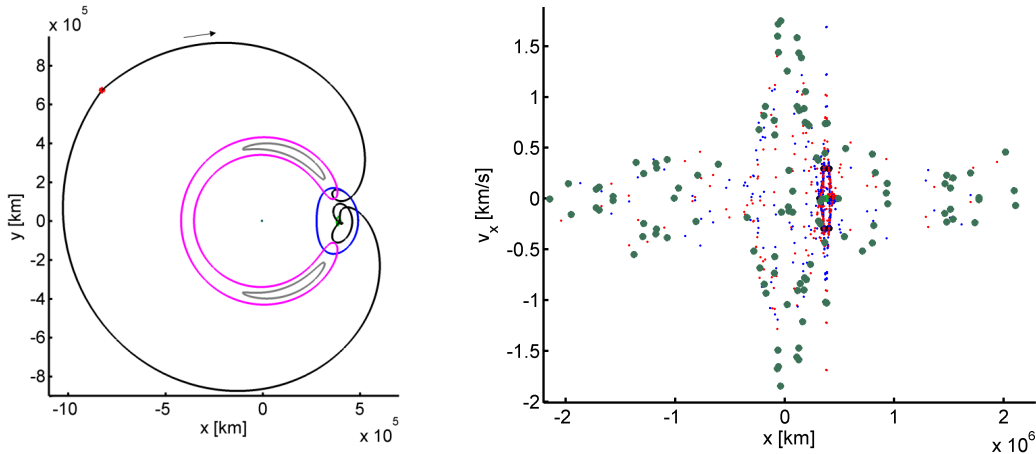


(a) Transfer from the 4:1 synodic resonant NRHO to a 20.97 day period DRO. (b) Transfer from the 4:1 synodic resonant NRHO to a 13.76 day period DRO.

Figure 20. Transfers from the 4:1 synodic resonant NRHO to various DROs.

Recall that constructing an initial guess for a transfer orbit is challenging because both the departure orbit (NRHO) and destination orbit (DRO) are effectively stable. However, it is observed that other orbits in the near-neighborhood of the DRO may be unstable and offer manifolds that can be exploited. One such nearby family is the Period-3 DRO (P3DRO) family, which evolves from the DRO family at a period-tripling bifurcation. The P3DROs, which possess similar Jacobi constant values to the DROs of interest, are unstable and therefore have stable and unstable manifolds. In

Figure 21(b), an $x-\dot{x}$ Poincaré map appears with the stable and unstable manifold crossings from a P3DRO (with a Jacobi constant value of 2.9992) at the $y = 0$ hyperplane. On this map, the red dots indicate crossings of the unstable P3DRO manifolds and the blue dots correspond to crossings of the stable P3DRO manifolds. A transfer, originating from the NRHO, to a 20.19 day period DRO is plotted in Figure 21(a) with a slightly more complex geometry; a loop appears in the second transfer segment prior to the DRO insertion. This transfer results in a total maneuver cost of 0.8966 km/s and a time of flight of 82.1 days. Propagating the second transfer segment from Figure 21(a) (between the intermediate and arrival maneuvers) forward and backward in time and plotting the crossings on the Poincaré map in Figure 21(b) demonstrates that this transfer shares similar characteristics to the P3DRO manifolds; thus, the P3DRO manifolds are useful for transfer design in this region.



(a) Transfer from the 4:1 synodic resonant NRHO to a 20.19 day period DRO.

(b) Poincaré map marking crossings of the transfer arc (green dots), the unstable manifold of the P3DRO (red dots), and the stable manifold of the P3DRO (blue dots).

Figure 21. This particular transfer geometry shares characteristics with the P3DRO manifolds.

STATIONKEEPING REVIEW

The feasibility of an Earth-Moon NRHO as a destination for a crewed spacecraft in a long-term orbit in cis-lunar space depends greatly on the ability to effectively stationkeep NRHOs over a long duration for a reasonable cost. An in-depth stationkeeping analysis for spacecraft in lunar NRHOs is summarized in Guzzetti et al.,⁶ with additional analysis provided in Davis et al.⁷ Two stationkeeping strategies are examined: a dynamical systems theory approach that exploits the understanding of the dynamics in the NRHO regime and a crossing-control algorithm in which a spacecraft state is targeted at a specific location a number of revolutions downstream.

The first NRHO stationkeeping strategy, termed the Cauchy-Green Tensor (CGT) targeting algorithm, employs a technique to estimate the downstream region that is attainable for a correction maneuver of a given magnitude. The CGT approach offers a nearly optimal stationkeeping maneuver that delivers the spacecraft as close as possible to a desired downstream reference state by leveraging an understanding of maneuver size and direction to maintain a perturbed orbit near a virtual reference orbit. Of particular note is the low computational cost associated with this strategy that renders it potentially suitable for on-board applications. The second strategy, termed the x -axis

crossing control algorithm, introduces a corrections maneuver to target the rotating x velocity, v_x , at a future time downstream. This scheme is used to test the feasibility of stationkeeping a noisy spacecraft with human-level disturbances. Stationkeeping the NRHOs with this method proves low-cost and effective. Analysis conducted for the Cauchy-Green Tensor targeting algorithm and the x -axis crossing control algorithm demonstrates that the NRHOs are viable candidates for a long-term inhabited spacecraft from a stationkeeping perspective—in the presence of varying levels of noise, NRHOs can be maintained over a long-duration for a low-cost using a variety of strategies.

FINAL REMARKS

The NRHOs, a subset of the L_1 and L_2 halo families of periodic orbits, are identified as viable candidate orbits for a habitat spacecraft in cis-lunar space. In this investigation, properties of the NRHOs that lead to their desirable characteristics are explored. These effectively stable periodic orbits possess favorable eclipse avoidance properties and can be transferred into a higher-fidelity ephemeris model for more in-depth mission analysis. As with any crewed mission, a capability to detect a diverging path is critical; the momentum integral offers one simple metric for this purpose. Additionally, preliminary transfer studies indicate that the NRHOs are accessible from LEO for a relatively low-cost and short time of flight, also a characteristic that is favorable for crewed missions. Investigation into accessing the DROs is conducted with preliminary results demonstrating that various dynamical structures in cis-lunar space can be useful for trajectory design. Ongoing investigations include alternative transfer geometries that exist between the NRHOs, DROs and other orbit families, eclipse avoidance techniques, and further understanding of this complex dynamical regime.

ACKNOWLEDGMENTS

This work was completed at Purdue University and NASA Johnson Space Center under contract #NNJ13HA01C. This work is supported in part by the Purdue University School of Aeronautics and Astronautics, as well as the Rune and Barbara Eliassen Visualization Laboratory. The authors would like to acknowledge Dr. Davide Guzzetti for previous contributions to the NRHO escape warning algorithm and other valuable discussions.

REFERENCES

- [1] B. Hufenbach, K. Laurini, N. Satoh, C. Lange, R. Martinez, J. Hill, M. Landgraf, and A. Bergamasco, “International Missions to Lunar Vicinity and Surface - Near-Term Mission Scenario of the Global Space Exploration Roadmap,” *IAF 66th International Astronautical Congress*, October 2015.
- [2] K. Laurini, B. Hufenbach, N. Satoh, J. Hill, and A. Ouellet, “The Global Exploration Roadmap and Expanding Human/Robotic Exploration Mission Collaboration Opportunities,” *IAF 66th International Astronautical Congress*, October 2015.
- [3] R. Whitley and R. Martinez, “Options for Staging Orbits in Cis-Lunar Space,” *IEEE Aerospace 2015*, March 2015.
- [4] K. Howell and J. Breakwell, “Almost Rectilinear Halo Orbits,” *Celestial Mechanics*, Vol. 32, No. 1, 1984, pp. 29–52.
- [5] I. Robin and V. Markellos, “Numerical Determinations of Three-Dimensional Orbits Generated from Vertical Self-Resonant Satellite Orbits,” *Celestial Mechanics*, Vol. 21, 1980, pp. 395–434.
- [6] D. Guzzetti, E. M. Zimovan, K. C. Howell, and D. C. Davis, “Stationkeeping Analysis for Spacecraft in Lunar Near Rectilinear Halo Orbits,” *Paper No. AAS-2017-395, AAS/AIAA Spaceflight Mechanics Meeting, San Antonio, Texas*, February 2017.
- [7] D. C. Davis, S. A. Bhatt, K. Howell, J. Jang, R. Whitley, F. Clark, D. Guzzetti, E. Zimovan, and G. Barton, “Orbit Maintenance and Navigation of Human Spacecraft at Cislunar Near Rectilinear Halo Orbits,” *Paper No. AAS 17-269, AAS/AIAA Spaceflight Mechanics Meeting, San Antonio, Texas*, February 2017.

- [8] J. Williams, D. E. Lee, R. L. Whitley, K. A. Bokelmann, D. C. Davis, and C. F. Berry, "Targeting Cis-lunar Near Rectilinear Halo Orbits for Human Space Exploration," *Paper No. AAS 17-267, AAS/AIAA Spaceflight Mechanics Meeting, San Antonio, Texas*, February 2017.
- [9] D. Grebow, M. Ozimek, K. Howell, and D. Folta, "Multi-Body Orbit Architectures for Lunar South Pole Coverage," *Journal of Spacecraft and Rockets*, Vol. 45, No. 2, 2008, pp. 348–358.
- [10] A. Haapala, *Trajectory Design in the Spatial Circular Restricted Three-Body Problem Exploiting Higher-Dimensional Poincaré Maps*. Ph.D. Dissertation, School of Aeronautics and Astronautics, Purdue University, West Lafayette, Indiana, December 2014.
- [11] D. Davis, S. Phillips, and B. McCarthy, "Multi-Body Mission Design Using the Deep Space Trajectory Explorer," *IAF 67th International Astronautical Congress, Guadalajara, Mexico*, September 26–30, 2016.
- [12] M. E. Stringer and D. L. Richardson, "An Investigation of A Family of 'Moon-Wrapping' Orbits About L_2 in the Earth-Moon Restricted 3-Body Problem," *Proceedings: Advances in the Astronautical Sciences*, Vol. 85, No. III, 1993, pp. 2431–2440.
- [13] L. Capdevila, D. Guzzetti, and K. Howell, "Various Transfer Options from Earth into Distant Retrograde Orbits in the Vicinity of the Moon," *AAS/AIAA Space Flight Mechanics Meeting, Santa Fe, New Mexico*, January 2014.
- [14] R. A. Broucke, "Periodic Orbits in the Restricted Three-Body Problem with Earth-Moon Masses," Technical Report, Jet Propulsion Laboratory, 1968.
- [15] M. Hénon, "Numerical Exploration of the Restricted Problem. VI: Hill's case: Non-Periodic Orbits," *Astronomy and Astrophysics*, Vol. 9, 1970, pp. 24–36.
- [16] M. Gates, D. Mazanek, B. Muirhead, S. Stich, B. Naasz, P. Chodas, M. McDonald, and J. Reuter, "NASA's Asteroid Redirect Mission Concept Development Summary," *Aerospace Conference, 2015, IEEE*, March 7-14, 2015.